

# Fluorine doping in dilute magnetic semiconductor $\text{Sn}_{1-x}\text{Fe}_x\text{O}_2$

Aaron Thurber · Jason Hays · K. M. Reddy ·  
V. Shutthanandan · Alex Punnoose

Received: 5 February 2007 / Accepted: 6 February 2007  
© Springer Science+Business Media, LLC

**Abstract** Recent studies have reported room-temperature ferromagnetism (FM) in Fe doped  $\text{SnO}_2$ . The FM in semiconductors due to transition metal doping has been argued to be carrier mediated. Fluorine (F) doping in pure  $\text{SnO}_2$  has been reported to significantly increase the carrier concentration. In this work, we investigated the role of F doping in the range from 0% to 0.79% on the FM of chemically synthesized single phase  $\text{Sn}_{1-x}\text{Fe}_x\text{O}_2$  using X-ray diffraction, UV-Vis spectrophotometry, particle-induced X-ray emission, particle-induced gamma ray emission and magnetometry. The saturation magnetization  $M_s$  (0.03 emu/g) increased by a factor of 2.5 and the lattice volume and band gap energy decreased by  $0.35 \text{ \AA}^3$  and 0.2 eV, respectively, with 0.67% F doping (F/Sn atom %) compared to the sample without any fluorine.

## 1 Introduction

Ferromagnetism in semiconductors has become an area of great interest for use in spintronics

---

IMRC 2006, Cancun Paper reference: S4-P50-Alex

---

A. Thurber · J. Hays · K. M. Reddy · A. Punnoose (✉)  
Department of Physics, Boise State University,  
Boise, ID 83725-1570, USA  
e-mail: apunnoos@boisestate.edu

V. Shutthanandan  
Environmental Molecular Sciences Laboratory,  
Pacific Northwest National Laboratory,  
Richland, WA 99352, USA

applications [1, 2]. One strong candidate for dilute magnetic semiconductors is  $\text{Sn}_{1-x}\text{Fe}_x\text{O}_2$ , as outlined in recent work [3, 4], showing above room-temperature ferromagnetism. However, the highest saturation magnetization  $M_s = 0.03 \text{ emu/g}$  ( $0.018 \mu_B/\text{Fe ion}$ ) obtained in these samples was fairly poor. For practical applications, the sample magnetization needs to be further improved. The origin of the ferromagnetic behavior has been argued to be carrier-mediated [5] and directly influenced by the charge carrier concentration. Rakhshani et al. [6] reported a significant increase in carrier concentration in the  $\text{SnO}_2$  system when doped with F. Therefore, we used additional fluorine doping in the  $\text{Sn}_{1-x}\text{Fe}_x\text{O}_2$  system to increase the carrier concentration and investigated the effects of varying fluorine concentrations on the physical properties of the system. There is also evidence that the magnetism produced by doping  $\text{SnO}_2$  with transition metals is related to changes in the chemical structure and crystal lattice [7, 8]. It has been shown that in itinerant electron metamagnets [9–11], ferromagnetism results from small changes in the internal pressure and lattice volume [3]. In this work, the  $\text{Sn}_{0.95}\text{Fe}_{0.05}\text{O}_2$  system was additionally doped with F as a means of increasing the carrier concentration of the semiconductor. Our studies show that changes in the magnetization of the material are directly related to fluorine doping concentration and presumably the consequent changes in the carrier concentration, although further tests are needed to offer more support for this argument. The sol-gel process was employed to synthesize powder samples for this study.

## 2 Experimental details

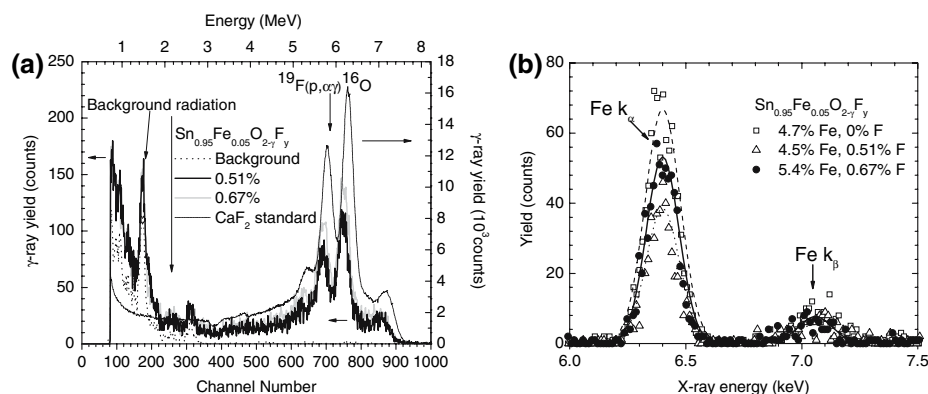
Using a synthesis process described elsewhere [3], varying amounts of HF were added during the reaction stage to produce  $\text{Sn}_{1-x}\text{Fe}_x\text{O}_2$  samples with a variation in F concentration and a target Fe concentration of 5%. The reaction precipitates were annealed at 600 °C. Samples prepared under identical conditions but without the tin chloride precursor resulted in hematite [3] and were used for comparison to the  $\text{Sn}_{1-x}\text{Fe}_x\text{O}_2$  samples as a means of ruling out the presence of impurity phases in the material. Particle-induced gamma ray emission (PIGE) and particle-induced X-ray emission (PIXE) were used to determine the F and Fe concentrations, respectively. The PIGE analysis was carried out using a  $^{19}\text{F}(p, \alpha\gamma)^{16}\text{O}$  nuclear reaction to probe the fluorine concentration. Samples were bombarded with a 1.2 MeV proton beam and the resulting gamma emission was measured with a bismuth germanium oxide detector. The amount of fluorine present was determined by calibrating the measurement against a  $\text{CaF}_2$  standard. PIXE and X-ray diffraction (XRD) studies were conducted as described elsewhere [3]. Diffuse reflectance data was recorded on a Cary 5000 spectrophotometer on powder samples packed into a horizontally mounted metal sample holder. A commercial magnetometer (Quantum Design, PPMS) equipped with a superconducting magnet was used to conduct magnetic measurements as a function of magnetic field (0 to  $\pm 65$  kOe). For the PPMS data, powder samples were tightly packed into a clear plastic straw.

## 3 Results

### 3.1 Particle-induced gamma ray and X-ray emission

Representative PIGE and PIXE spectra are shown in Fig. 1. In Fig. 1a, spectra for two samples are shown,

**Fig. 1** (a) PIGE for a  $\text{CaF}_2$  standard, system background radiation, 0.51% and 0.67% F doped  $\text{Sn}_{0.95}\text{Fe}_{0.05}\text{O}_2$  samples and (b) PIXE for 0%, 0.51% and 0.67% F doped  $\text{Sn}_{0.95}\text{Fe}_{0.05}\text{O}_2$



giving a variation in F content. A  $\text{CaF}_2$  standard was used as a reference to estimate the F concentration in the sample after subtracting the background data (see Fig. 1a). The Fe  $K_\alpha$  and  $K_\beta$  regions obtained from PIXE are shown in Fig. 1b, demonstrating the small differences in Fe concentration verifying the nominal dopant concentration of  $\sim 5\%$ . The estimated concentrations of both F and Fe for each sample are outlined in Table 1.

### 3.2 X-ray diffraction

XRD spectra showed strong tetragonal  $\text{SnO}_2$  peaks with weaker orthorhombic peaks, as seen in Fig. 2. Also shown are the expected positions for the orthorhombic phase and cassiterite form of  $\text{SnO}_2$  as well as those for romarchite  $\text{SnO}$ . Clearly, cassiterite is the dominant phase mixed with a small degree of the metastable orthorhombic phase. The hematite lines do not appear in any of the spectra and rule out the formation of these iron oxides to the detectability limit of the XRD ( $\sim 1.5\%$ ) [3]. Results of analyzing the XRD spectra are shown in Fig. 3 and Table 1. The average crystallite size estimated using the (101) and (202) peaks increased from 164 Å to 261 Å for 0.67% F over the sample without fluorine (See Fig. 3a). The lattice volume (Fig. 3a) revealed a maximum level of lattice contraction for 0.67% F doping, decreasing from 71.2 Å<sup>3</sup> to 70.8 Å<sup>3</sup>. This may be due to the substitution of 1.3 Å radius F ions at the sites of 1.4 Å radius O ions. Fig. 3b demonstrates that the change in tetragonal lattice parameter  $a$  is more pronounced than the changes in parameter  $c$ , indicating that the co-incorporation of the dopants results in stretching or compressing of the lattice primarily in the  $a$ -direction, altering the tetragonality of the lattice. Figure 4c shows the orthorhombic fraction [7] steadily decreasing as fluorine is introduced into the system. This is an important effect since in Fe doped  $\text{SnO}_2$  samples investigated earlier [3], the orthorhombic phase

**Table 1** Concentrations of Fe and F dopants within SnO<sub>2</sub> and the resulting physical properties

Fe% from PIXE	F% from PIGE	Lattice volume (Å <sup>3</sup> )	Band gap (eV)	Orthorhombic phase fraction	Saturation magnetization M <sub>s</sub> (emu/g)	Remanence M <sub>r</sub> (emu/g)	Coercivity H <sub>c</sub> (Oe)
0	0	71.42	3.60	0.12	–	–	–
4.7	0	71.20	2.75	0.39	0.03	0.0048	53
4.5	0.51	71.15	2.74	0.16	0.063	0.0069	29
5.4	0.67	70.85	2.55	0.11	0.076	0.0073	30
4.8	0.79	71.16	3.02	0.05	0.013	0.003	49

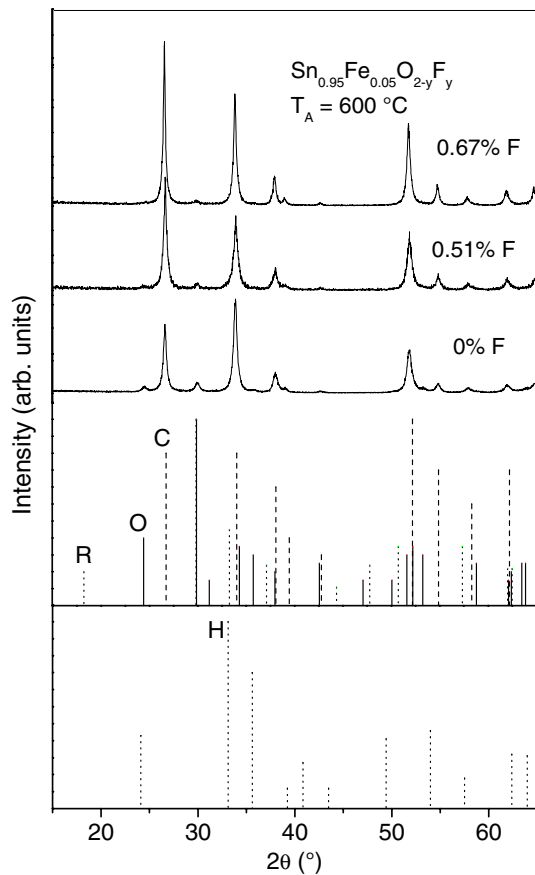


**Fig. 2** XRD spectra of Sn<sub>0.95</sub>Fe<sub>0.05</sub>O<sub>2-y</sub>F<sub>y</sub> samples with reference lines of orthorhombic SnO<sub>2</sub> (marked O), romarchite SnO (marked R), and cassiterite SnO<sub>2</sub> (marked C) phases and hematite (marked H)

fraction steadily increased with Fe doping concentration suggesting the possibility that the orthorhombic SnO<sub>2</sub> phase may be responsible for the observed ferromagnetism. The observed decrease in the orthorhombic phase fraction with F doping will allow us to determine if this phase is responsible for the observed ferromagnetism in these powders, as discussed in the following sections. The orthorhombic phase has been primarily observed in nanoparticles and thin films which are expected to have a large number of defects. The systematic decrease in the orthorhombic phase

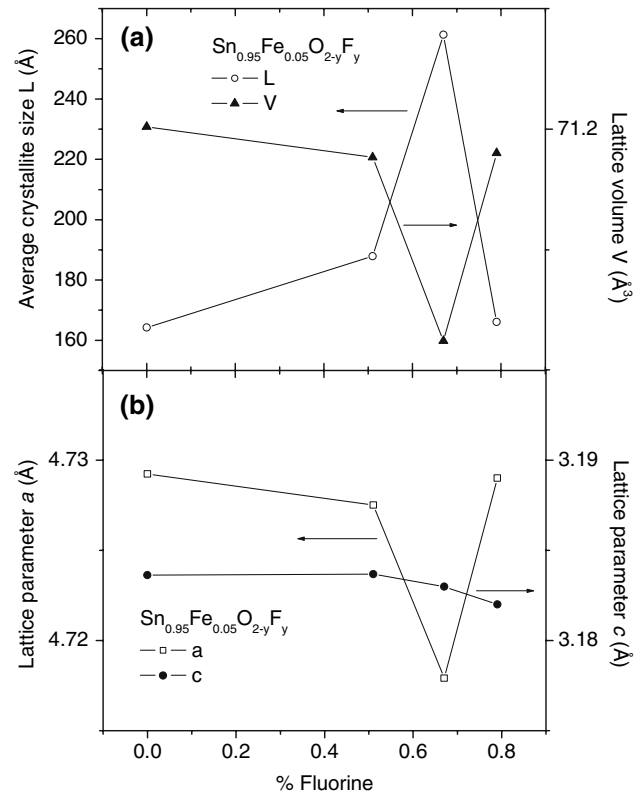


**Fig. 3** (a) Changes in average crystallite sizes estimated from XRD and lattice volume and (b) tetragonal lattice parameters *a* and *c* of Sn<sub>0.95</sub>Fe<sub>0.05</sub>O<sub>2</sub> powders as a function of fluorine concentration

fraction with F concentration, shown in Table 1 and Fig. 4c, might indicate a decreasing defect concentration and/or improvement in the lattice structure.

### 3.3 Optical measurements

Figure 4a shows diffuse reflectance for pure SnO<sub>2</sub>, a 5% hematite/cassiterite physical mixture and pure hematite and Fig. 4b shows the same for 0%, 0.67% and 0.51% F doped Sn<sub>0.95</sub>Fe<sub>0.05</sub>O<sub>2</sub> powder samples. The absence of the characteristic absorption feature at 550 nm of the hematite sample in the Sn<sub>0.95</sub>Fe<sub>0.05</sub>O<sub>2</sub> samples with and without F in Fig. 4b helps rule out

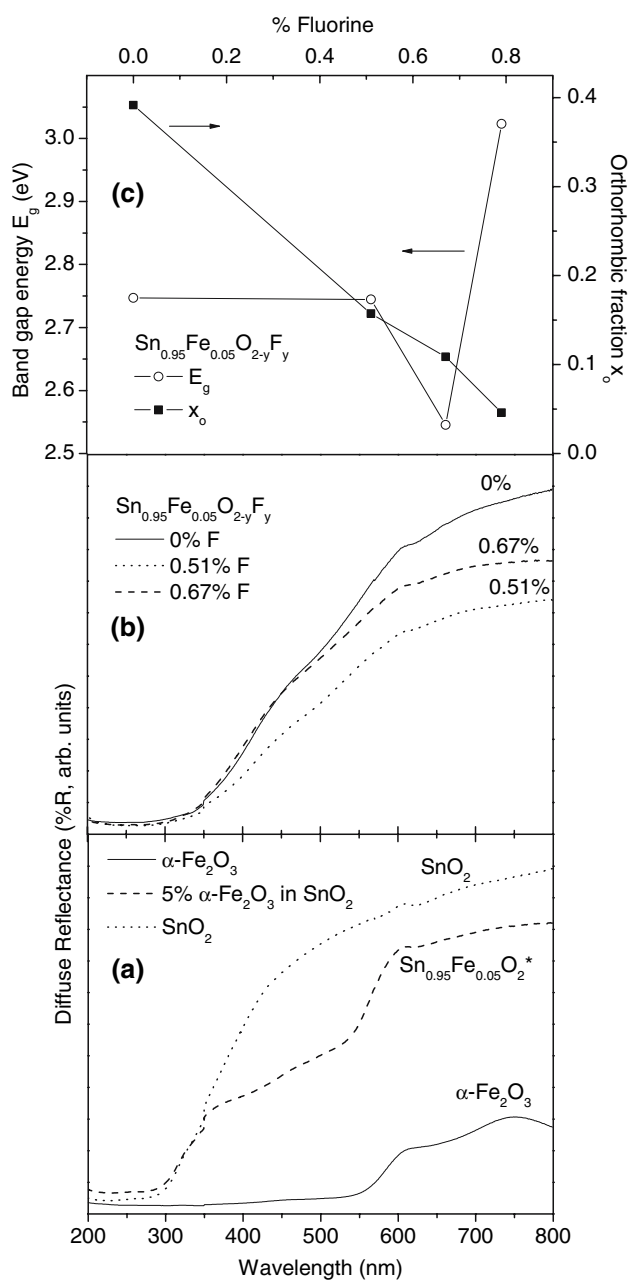


**Fig. 4** (a) Diffuse reflectance of pure  $\text{SnO}_2$  powder, a 5% hematite/cassiterite physical mixture and that of pure hematite, (b) diffuse reflectance of 0.51% and 0.67% F doped  $\text{Sn}_{0.95}\text{Fe}_{0.05}\text{O}_2$  and (c) band gap energy  $E_g$  estimated from diffuse reflectance and orthorhombic fraction  $x_0$  determined from XRD as a function of fluorine concentration

the presence of hematite within the powders. The variation of the band gap energies determined using the Kubelka–Munk function  $F(R) = (1-R)^2/2R$ , shown in Fig. 4c, give a minimum of 2.55 eV for 0.67% F doping, down from 2.75 eV for the  $\text{Sn}_{0.95}\text{Fe}_{0.05}\text{O}_2$  sample without fluorine. For all of the samples investigated, the band gap energies were much lower than

the expected 3.6 eV for bulk pure  $\text{SnO}_2$ , ranging from 2.55 eV to 3.02 eV.

### 3.4 Magnetic measurements

$M$  versus  $H$  data recorded at room temperature shown in Fig. 5a reveal that samples have a linear paramagnetic component  $\chi_p$  [3] superimposed on a ferromagnetic-like saturation. The resulting magnetization after subtracting the linear paramagnetic susceptibility  $\chi_p$  is shown in Fig. 5b. The saturation magnetization of the  $\text{Sn}_{0.95}\text{Fe}_{0.05}\text{O}_2$  sample is increased by a factor of 2.5 with 0.67% F doping, shown in Fig. 6. This suggests that the ferromagnetism in this system is controlled by the F dopant concentration and the resulting changes in the carrier concentration and/or lattice volume and electronic structure of the material. The F concentration of 0.51% had a similar effect on the saturation and remanent magnetizations as 0.67% doping. Magnetic remanence, in general, followed the same trend as the

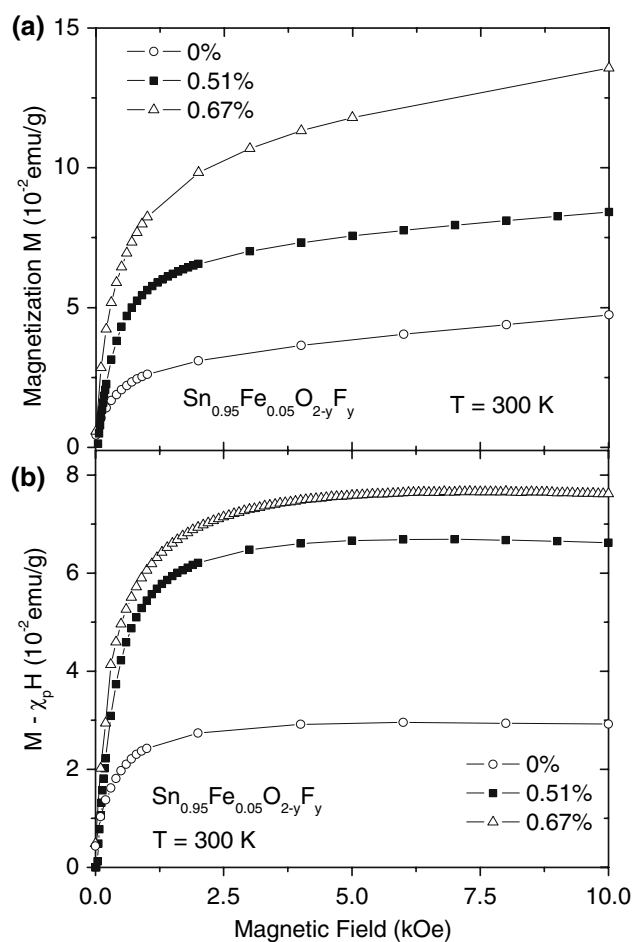


**Fig. 5** (a) Room-temperature  $M$  versus  $H$  of 0%, 0.51% and 0.67% F doped  $\text{Sn}_{0.95}\text{Fe}_{0.05}\text{O}_2$  and (b)  $M - \chi_p$  versus  $H$  of same, obtained by subtracting the linear component

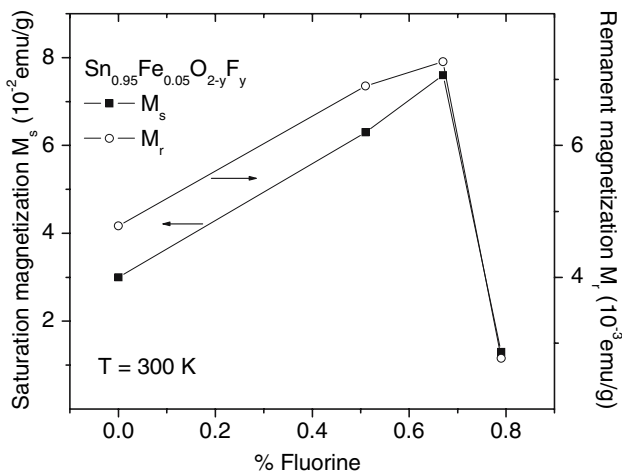


**Fig. 6** Saturation magnetization  $M_s$  and remanent magnetization  $M_r$  of  $\text{Sn}_{0.95}\text{Fe}_{0.05}\text{O}_2$  powders as a function of fluorine concentration

saturation magnetization for each sample (Fig 6). However, for the 0.79% F doped samples, the overall magnetic moment decreases significantly. A similar reverse effect was also observed in the lattice volume and band gap, thus indicating that F doping above 0.67% disturbed the ferromagnetic interaction probably due to the changes and disorder in the lattice structure, although a complete understanding of the actual reason behind this change needs more investigations. The F doped  $\text{Sn}_{1-x}\text{Fe}_x\text{O}_2$  samples showed coercivity ranging from 30 Oe to 53 Oe.

#### 4 Conclusions

Additional dilute fluorine doping into the  $\text{Sn}_{1-x}\text{Fe}_x\text{O}_2$  system has drastic effects on the structural, optical and magnetic properties of the material. The ferromagnetism in  $\text{Sn}_{0.95}\text{Fe}_{0.05}\text{O}_2$  was successfully enhanced by the addition of fluorine into the system. The ferromagnetic parameters  $M_s$ ,  $M_r$  and  $H_c$ , the band gap energy  $E_g$  and crystal lattice parameters are all modified when adding varying fluorine concentrations. No impurities were detected in any of the samples investigated. The carrier

concentration of tin dioxide is expected to increase with fluorine doping and the enhanced ferromagnetism observed in our fluorine doped  $\text{Sn}_{0.95}\text{Fe}_{0.05}\text{O}_2$  samples might indicate that the ferromagnetism may be carrier-mediated. However, to confirm this, detailed electrical studies including anomalous Hall effect measurements are necessary, which will be undertaken in the future. The results also show that the dominant cassiterite  $\text{SnO}_2$  phase, and not the weaker orthorhombic  $\text{SnO}_2$  phase fraction, is responsible for the ferromagnetic behavior in  $\text{Sn}_{1-x}\text{Fe}_x\text{O}_2$ .

**Acknowledgements** This research was supported in part by grants from Petroleum Research Fund (AC grant, PRF#41870-AC10), National Science Foundation (DMR-MRI grant; NSF-Idaho-EPSCoR program (EPS-0447689); NSF-CAREER program (DMR-0449639)) and the Department of Energy (DoE-EPSCoR program (DE-FG02-04ER46142)). A portion of the research described in this paper was performed in the Environmental Molecular Sciences Laboratory, a national scientific user facility sponsored by the Department of Energy's Office of Biological and Environmental Research located at Pacific Northwest National Laboratory.

#### References

1. G.A. Prinz, *Science*, **282**, 1660 (1998); D.D. Awschalom, J.M. Kikkawa, *Phys. Today*, **52**, 33 (1999)
2. S.A. Chambers, R.F.C. Farrow, *MRS Bull.* **28**, 729 (2003); W. Prellier, A. Fouchet, B. Mercey, *J. Phys.: Condens. Matter* **15**, R1583 (2003); S. Picozzi, *Nat. Mater.* **3**, 349 (2004)
3. A. Punnoose, J. Hays, A. Thurber, M.H. Engelhard, R.K. Kukkadapu, C. Wang, V. Shutthanandan, S. Thevuthasan, *Phys. Rev. B* **72**, 054402 (2005)
4. X. Mathew, J. Hays, C. Mejía-García, G. Contreras-Puente, A. Punnoose, *J. Appl. Phys.* **99**, 08M101 (2006)
5. T. Dietl, H. Ohno, F. Matsukura, *Phys. Rev. B* **63**, 195205 (2001)
6. A.E. Rakhshani, Y. Makdisi, H.A. Ramazaniyan, *J. Appl. Phys.* **83**, 1049 (1998)
7. J. Hays, A. Punnoose, R. Baldner, M.H. Engelhard, J. Peloquin, K.M. Reddy, *Phys. Rev. B* **72**, 075203 (2005)
8. A. Punnoose, J. Hays, *J. Appl. Phys.* **97**, 10D321 (2005)
9. N.H. Duc, T. Goto in *Handbook on the Physics and Chemistry of Rare Earths*, vol. 26, ed. by K.A. Gschneidner Jr., L. Eyring (Elsevier, 1999) pp. 178
10. T. Goto, K. Fukamichi, H. Yamada, *Physica B* **300**, 167 (2001)
11. E.P. Wohlfarth, P. Rhodes, *Philos. Mag.* **7**, 1817 (1962)